Journal of Power Sources 196 (2011) 3083–3088

Contents lists available at ScienceDirect

Journal of Power Sources

journal homepage: www.elsevier.com/locate/jpowsour

Assessment of perovskite-type $La_{0.8}Sr_{0.2}Sc_xMn_{1-x}O_{3-\delta}$ oxides as anodes for intermediate-temperature solid oxide fuel cells using hydrocarbon fuels

S. Sengodan [a], H.J. Yeo [a], J.Y. Shin [b], G. Kim [a,*]

[a] Interdisciplinary School of Green Energy, Ulsan National Institute of Science and Technology (UNIST), Ulsan 689-798, Republic of Korea
[b] Department of Mechanical Engineering, Dong-Eui University, Busan 614-714, Republic of Korea

ARTICLE INFO

Article history:
Received 7 October 2010
Received in revised form
15 November 2010
Accepted 17 November 2010
Available online 8 December 2010

Keywords:
Intermediate-temperature solid oxide fuel cells
Ceramic anode
Perovskite
Oxygen non-stoichiometry
Hydrocarbon

ABSTRACT

Composites formed by the infiltration of 40 wt% $La_{0.8}Sr_{0.2}Sc_xMn_{1-x}O_{3-\delta}$ (LSSM) oxides ($x = 0.1, 0.2, 0.3$) into 65% porous yttria-stabilized zirconia (YSZ) are investigated as anode materials for intermediate-temperature solid oxide fuel cells for hydrocarbon oxidation. The oxygen non-stoichiometry and electrical conductivity of each LSSM–YSZ composite are determined by coulometric titration. As the concentration of Sc increases, the composites show higher phase stability and the electrical conductivity of LSSM is significantly affected by the Sc doping, the non-stoichiometric oxygen content, and oxygen partial pressure ($p(O_2)$). To achieve better electrochemical performance, it is necessary to add ceria-supported palladium catalyst for operation with humidified CH_4. Anode polarization resistance increases with Sc doping due to a decrease in electrical conductivity. An electrolyte-supported cell with a LSSM–YSZ composite anode delivers peak power densities of 395 and 340 mW cm^{-2} at 923 K in humidified (3% H_2O) H_2 and CH_4, respectively, at a flow rate of 20 mL min^{-1}.

1. Introduction

A fuel cell is a flexible electrochemical device, which converts chemical energy directly into electrical energy with high efficiency and low pollutants. Solid oxide fuel cells (SOFCs) and polymer electrolyte membrane fuel cells (PEMFCs) have received most attention in past decades. Compared with other types of fuel cell, SOFCs are widely studied because of advantages such as fuel flexibility along with high tolerance to impurities in the fuel and the fact that expensive noble metal catalysts are not required. State of the art Ni based SOFC anodes are, however, limited to hydrogen fuel due to carbon deposition on the Ni anode in the presence of dry hydrocarbons [1,2].

Recently much effort has been devoted to developing intermediate temperature solid oxide fuel cells (IT-SOFCs) that operate with hydrocarbon fuels at a working temperature around 873–1073 K [3,4]. In the past 20 years, many materials have been evaluated as candidates for the anode to give the efficient operation of IT-SOFCs. Anodes of IT-SOFCs have to overcome many problems such as easy poisoning by sulphur, carbon deposition, and the poor reduction–oxidation stability of existing nickel anodes in conventional SOFCs equipped with reformer. The anodes should also be chemically and mechanically stable under SOFC operating conditions. High ionic and electronic conductive phases with proper porosity, good catalytic properties, and a matching thermal expansion coefficient to electrolyte over a wide $p(O_2)$ range are also required. One of the well-known feasible ways to meet this need is to develop perovskite-based anodes. In this context, several perovskite type (ABO_3) composite materials have been explored as potential SOFC anodes for converting hydrocarbons to electrical energy, and that are tolerant to gas impurities without the addition of steam.

It has been reported that IT-SOFCs with a perovskite-YSZ conductive composite, e.g., $La_{0.75}Sr_{0.25}Cr_{0.5}Mn_{0.5}O_3$ (LSCM) or $La_{0.3}Sr_{0.7}TiO_3$ (LST), as an anode and YSZ as an electrolyte show promising electrocatalytic activity and electrical conductivity Kim et al. [5,6] reported potential findings for composite anodes based on infiltration of LSCM and LST. LSCM is a *p*-type conductor with a conductivity of 38 S cm^{-1} in air and 1.5 S cm^{-1} in 5% H_2 at 1173 K [3,7]. LST has been known to have conductivities greater than 20 S cm^{-1} at 973 K under anode operating conditions [8]. Both LSCM and LST show outstanding anode performances associated with the infiltration of LSCM and LST into porous YSZ. The composites prepared by the infiltration have long triple-phase boundary (TPB) lengths due to a process that involves spreading of the ceramic under oxidizing conditions followed by fracturing under reducing conditions [9].

Doping has been widely used to change the properties of $La_{0.8}Sr_{0.2}MnO_3$ (LSM) and Sc^{3+} has been reported as an outstanding dopant for perovskites [10,11]. Zheng et al. [12] have recently

* Corresponding author. Tel.: +82 52 217 2917; fax: +82 52 217 2909.
E-mail address: gtkim@unist.ac.kr (G. Kim).

0378-7753/$ – see front matter © 2010 Elsevier B.V. All rights reserved.
doi:10.1016/j.jpowsour.2010.11.161

demonstrated $La_{0.8}Sr_{0.2}Sc_xMn_{1-x}O_{3-\delta}$ (LSSM) as an electrode for symmetric SOFCs. As the anode material, $La_{0.8}Sr_{0.2}Sc_{0.2}Mn_{0.8}O_3$ shows good chemical and structural stabilities with an electrical conductivity of 5.2 S cm^{-1} in dry H_2/Ar at 1123 K, a value that is somewhat higher than that of LSCM (1.02 S cm^{-1}) under dry hydrogen. This LSSM oxide when used as the anode in a symmetric fuel cell performed reasonably well; it displayed significant redox stability in methane fuel without carbon deposition and had an area specific resistance (ASR) of 0.81 Ω cm^2 and a power density of 310 and 130 mW cm^{-2} under H_2 and CH_4 as fuels at 1173 K, respectively [12].

In this communication, an LSSM–YSZ composite has been prepared and evaluated as an anode for a IT-SOFC via the infiltration method. The fabrication procedure and performance of an electrolyte-supported cell with a ($La_{0.8}Sr_{0.2}FeO_3$)–YSZ composite cathode are investigated to assess the feasibility of LSSM–YSZ composites as an alternative anode material. In addition, the oxygen isotherms and electrical characteristics are evaluated by coulometric titration and four-probe techniques, respectively.

2. Experimental procedures

A three-layer wafer was made by tape casting, with the outer two layers having pore formers. A dense YSZ slurry was prepared by mixing YSZ powder (Tosoh-Zirconia, TZ-8Y, Tosoh Corp.) in distilled water, into which a dispersant (Durmax D 3005 polymer, Rohm & Haas), and binders (HA 12 and B 1000, Rohm & Haas) were added. Porous YSZ was prepared by adding YSZ powder (Tosoh-Zirconia, TZ-8Y, Tosoh Corp.), dispersant (Durmax D 3005 polymer, Rohm & Haas), binders (HA 12 and B 1000, Rohm & Haas) and graphite (UCP-2 grade, Alfa Aesar) sequentially to distilled water. The resultant two slurries were tape-casted separately. The porous–dense–porous YSZ structure was prepared by laminating three green tapes, followed by sintering at 1773 K for 4 h, after which the porosity was approximately 65%. The final thicknesses of the dense electrolyte and porous electrode were 85 and 50 μm, respectively.

A LSSM–YSZ anode was prepared by infiltrating LSSM oxide into the anode side of three-layered YSZ backbone composites. Nitrate salts of La, Sr, Sc and Mn were dissolved in water at a molar ratio of 0.8:0.2:0.1:0.9 (LSS01M), 0.8:0.2:0.2:0.8 (LSS02M), and 0.8:0.2:0.3:0.7 (LSS03M), respectively, along with citric acid. The concentration of the citrate ion was in a one-to-one mole ratio with the metal ion. LSSM was infiltrated into YSZ by means of a multi-step process that was followed by heating at 723 K to decompose the nitrates and citric acid. Infiltration was repeated until the desired loading of oxide was achieved. Finally the wafer was heated in air at 1123 K to obtain the perovskite phase. The LSF ($La_{0.8}Sr_{0.2}FeO_3$)–YSZ cathode was synthesized via the same procedure, i.e., infiltration with aqueous solution of $La(NO_3)_3{\cdot}6H_2O$, $Sr(NO_3)_2$ and $Fe(NO_3)_3{\cdot}9H_2O$ was followed by heating in air at 1123 K. 1 wt% Pd and 10 wt% ceria were also infiltrated into the anode and 1 wt% Pd into the cathode as catalysts [13] and heated in air at 723 K, to evaluate the effects of the catalysts according to the fuels.

For fuel cell performance tests, the cells were mounted on alumina tubes with ceramic adhesives (Ceramabond 522, Aremco). Silver paste and silver wire were used for electrical connections to both the anode and the cathode. The entire cell was placed inside a furnace and heated to the desired temperature. The anode was exposed to humidified (3% H_2O) CH_4 and H_2 at a flow rate of 20 mL min^{-1} and the cathode was left open in air. Impedance spectra and *V–i* polarization curves were measured using a BioLogic Potentiostat. Impedance spectra were measured galvanostatically at various currents in the frequency range of 500 kHz–1 mHz, with an a.c. perturbation of 10 mA.

Coulometric titration (CT) was used to quantify the oxidation/reduction state of the LSSM–YSZ composites, which has been described in more detail elsewhere [14]. Electrical conductivity of the composites was measured as a function of $p(O_2)$ using the standard four-probe technique. Samples for CT and conductivity measurement were prepared by the infiltration of LSSM into a porous YSZ slab, 2.2 mm × 5.3 mm × 9.9 mm in size. The composites were characterized by X-ray diffraction (XRD) and scanning electron microscopy (SEM).

3. Results and discussion

3.1. Microstructure and stability

The microstructure, porosity of the electrodes, physical binding between the electrodes and electrolyte, and cell processing are important determinants of cell performance even though the material itself has a good electrochemical and electrocatalytic activities. X-ray diffraction and scanning electron microscopy were employed to understand the structure and morphology of the LSSM–YSZ composites.

The XRD patterns of a 40% LSSM–YSZ composite calcined at 1123 K for 4 h in air are presented in Fig. 1. All the XRD measurements were performed on electrolyte-supported cell. Anode

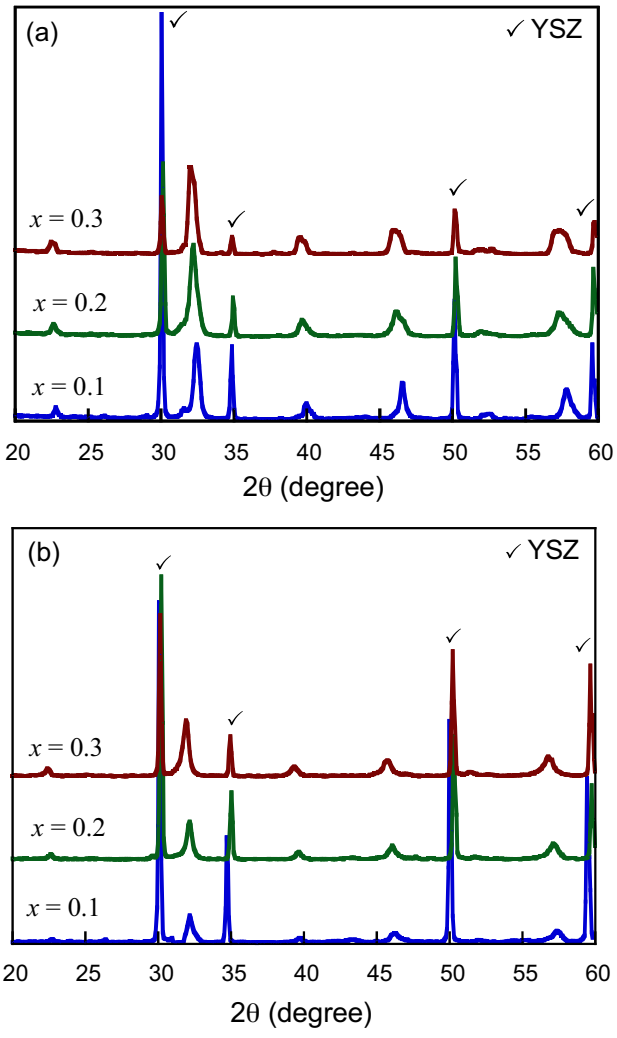

Fig. 1. XRD patterns of $La_{0.8}Sr_{0.2}Sc_xMn_{1-x}O_{3-\delta}$–YSZ ($x$ = 0.1, 0.2, 0.3) (a) composite calcined at 1123 K for 4 h in air and (b) composite after treatment with H_2 at 973 K for 4 h.

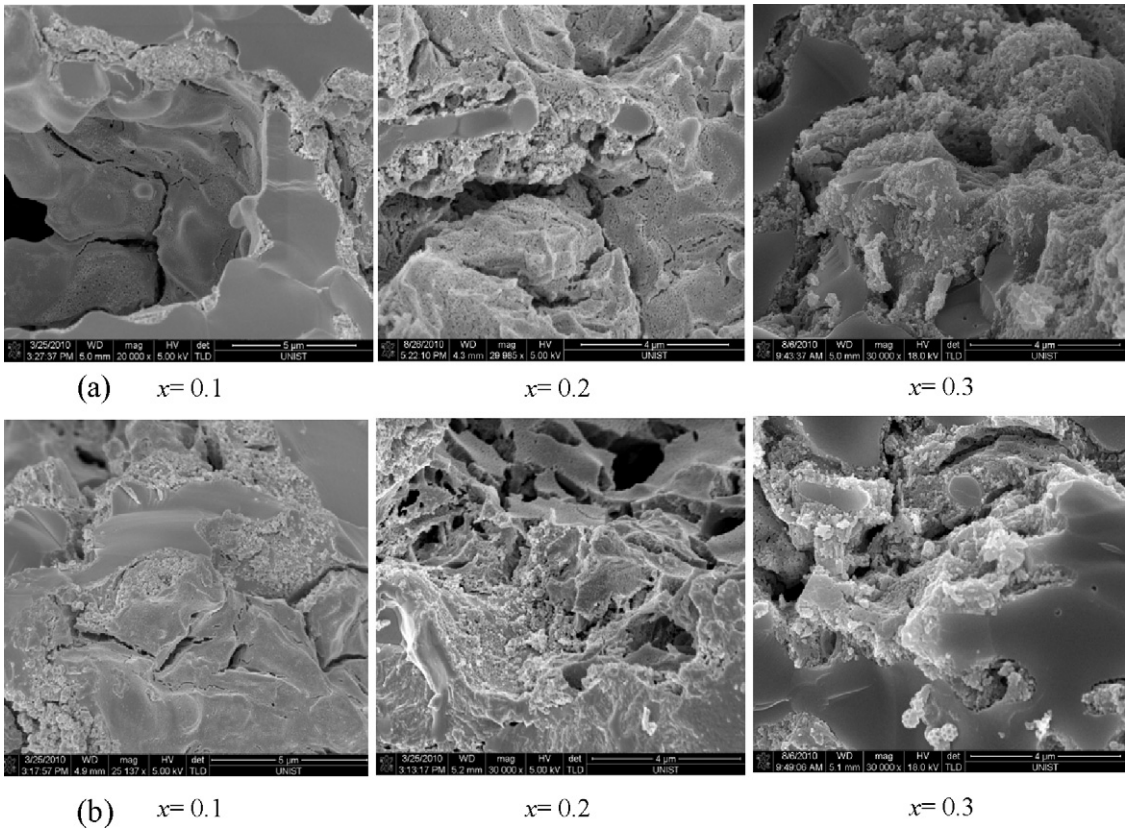

Fig. 2. A high-resolution SEM images of $La_{0.8}Sr_{0.2}Sc_xMn_{1-x}O_{3-\delta}$–YSZ ($x = 0.1, 0.2, 0.3$) (a) composites with LSSM calcined at 1123 K for 4 h in air and (b) same composites after reduction in humidified H_2 at 973 K for 4 h.

material should have high chemical, structural, and morphological stabilities under working conditions of an IT-SOFC, i.e., low $p(O_2)$. The patterns clearly demonstrate that all LSSM–YSZ composite anodes retain a stable pervoskite lattice structure, which is produced from the decomposition of the nitrate precursor solution. The XRD patterns of $La_{0.8}Sr_{0.2}Sc_xMn_{1-x}O_{3-\delta}$ ($x = 0.1, 0.2, 0.3$) after treatment with H_2 at 973 K for 4 h are also shown in Fig. 1. The formed pervoskite structure is still stable after being treated in a highly reducing atmosphere. No additional diffraction peaks are observed and this indicates that the perovskite structure is successfully preserved even after deep reduction.

SEM images of LSSM–YSZ composites after calcination at 1123 K for 4 h in air and at 973 K for 4 h in H_2 are presented in Fig. 2. There are no significant changes in the microstructure of the electrode before and after reduction. In general, the good wettability of oxide over YSZ ensures a good interconnection for electrical conduction, which minimizes the ohmic losses in the composite electrodes. Such a uniform interconnection was observed in the LSSM oxide but this uniformity became weaker with a higher amount of Sc doping.

3.2. Oxygen non-stoichiometry and electrical conductivity

The dependence of the oxygen deficiency of LSSM in the composite structure was determined by coulometric titration as a function of $p(O_2)$ at a temperature of 973 K with 37% LSSM–YSZ composites. The oxygen stoichiometries shown in Fig. 3 were obtained through CT experiments after passing a 5% H_2–95% Ar mixture. There is a considerable change in the oxygen stoichiometry (δ) throughout the whole $p(O_2)$ range.

The data indicate that the reduction–oxidation behaviour of LSSMs ($x = 0.1, 0.2, 0.3$) is similar for a highly reduced state at each temperature. The equilibrium property of LSM is included from the literature [15] for comparison purposes. The lattice oxygen in LSM is reduced much more rapidly with decreasing $p(O_2)$. The removal of lattice oxygen from the composites in the low $p(O_2)$ region results in the formation of oxygen vacancies and partial reduction of Mn to match the neutrality. Mn reduction from Mn^{4+} to Mn^{3+} occurs under anode operating conditions and is partially stabilized by Sc^{3+}in LSSM simply minimizing the extent of reduction and therefore stabilizing the structure to low $p(O_2)$ [12]. Under anode operating conditions, the oxygen non-stoichiometry for LSS01M is around 2.84.

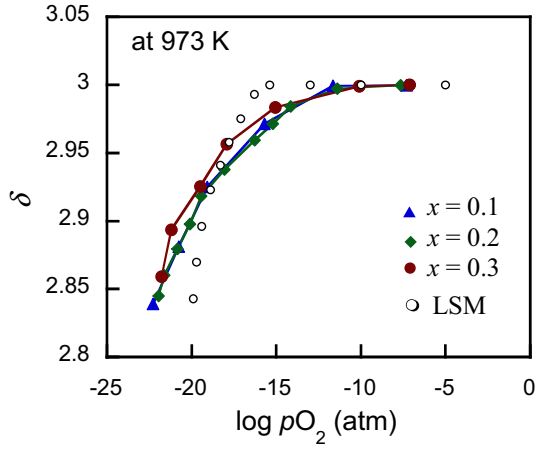

Fig. 3. Equilibrium oxygen stoichiometries measured using coulometric titration at 973 K for 37 wt% $La_{0.8}Sr_{0.2}Sc_xMn_{1-x}O_{3-\delta}$–YSZ ($x = 0.1, 0.2, 0.3$).
Data for bulk $La_{0.8}Sr_{0.2}MnO_{3-\delta}$ (○: LSM) from Ref. [15] shown for comparison.

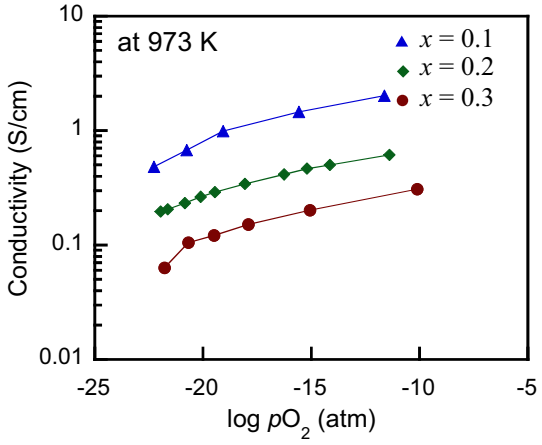

Fig. 4. Electrical conductivity obtained using 4-probe measurements for 37 wt% $La_{0.8}Sr_{0.2}Sc_xMn_{1-x}O_{3-\delta}$–YSZ($x$ = 0.1, 0.2, 0.3) composite as function of $p(O_2)$ at 973 K. $p(O_2)$ was controlled and measured using the coulometric-titration apparatus.

The electrical conductivities of LSSM-YSZ composites are shown in Fig. 4 as a function of $p(O_2)$ at 973 K. LSS01M demonstrates a maximum conductivity of 0.48 S cm^{-1} at a $p(O_2)$ around 10^{-23} atm. LSS02M shows 0.19 S cm^{-1} at $p(O_2)$ around 10^{-22} atm and LSS03M shows 0.06 S cm^{-1} at $p(O_2)$ of around 10^{-22} atm, respectively. At lower $p(O_2)$, removal of lattice oxygen leads to the formation of oxygen vacancies and partial reduction of Mn^{4+} to Mn^{3+}, which inhibits the electron hopping conduction mechanism to a certain degree [12] and partly explains the low electrical conductivity at low $p(O_2)$, It is also seen that the electrical conductivity decreases with a higher Sc doping level. It seems that the constant valence state of Sc^{3+} in LSSM inhibits electron conduction between oxygen and Mn and, hence, Sc may act as a block for the electron conduction [16]. This can be identified in Fig. 4 which shows decreasing conductivity with increasing Sc doping. The overall conductivity is enhanced at higher $p(O_2)$, which indicates that this material is p-type electronic conductor.

3.3. *V–i* polarization curve

To demonstrate the performance of the LSSM–YSZ composite anode, single cells with the configuration LSSM–YSZ/YSZ/LSF–YSZ were fabricated. The *V–i* polarization curve in humidified H_2 and CH_4, is given in Figs. 5 and 6, respectively. The open-circuit voltage is near the theoretical Nernst potential, viz., 1.1 V and the *V–i* relationships were nearly linear indicating that a reasonably gas tight sealing and gas-tight dense YSZ are formed. The maximum peak power density is 395 and 341 mW cm^{-2} (LSS01M) in H_2 and CH_4, respectively, at 973 K. The power density of the cell decreases with Sc doping. The corresponding impedance data at OCV are shown in Fig. 7. The high frequency offset is due mainly to the electrolyte resistance, and the difference between high and low frequency intercepts with the real axis is associated with the electrode contribution. An identically arranged single cell was employed for all LSSMs (x = 0.1, 0.2, 0.3) single cells. The ohmic losses for LSS01M and LSS02M are about 0.45 Ω cm^2, which are in good agreement with the expected ohmic losses associated with 85 μm thickness electrolyte [17]. There is a difference in the non-ohmic losses for LSS01M and LSS02M, i.e., 0.5 and 0.65 Ω cm^2 for methane fuel, respectively. The lower non-ohmic losses of LSS01M are attributed to the fact that the anode polarization resistance of LSS01M is lower than that of LSS02M. Nevertheless, the large difference in ohmic losses compared with LSS03M (about 0.7 Ω cm^2) is thought to originate from the inadequate conductivity of LSS03M, 0.06 S cm^{-1} at $p(O_2)$ of around 10^{-22} atm at 973 K. The electrochemical impedance

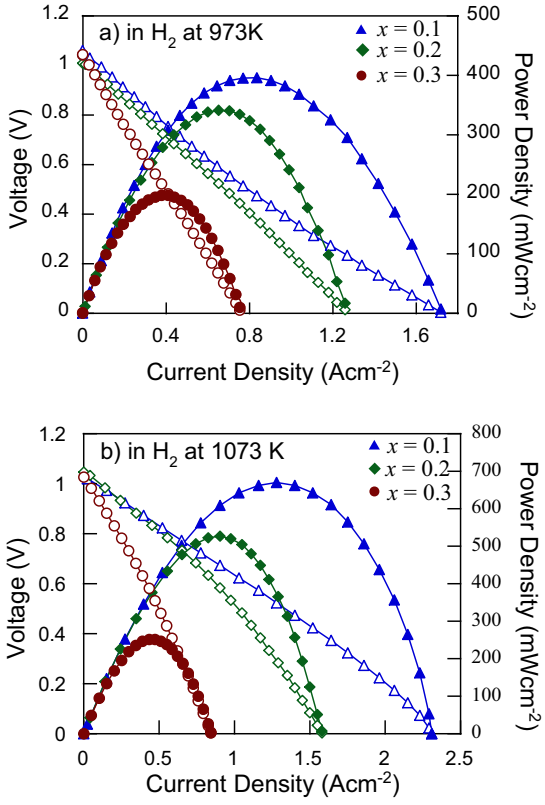

Fig. 5. *V–i* polarization curves for cells having anode prepared by infiltration of 40 wt% $La_{0.8}Sr_{0.2}Sc_xMn_{1-x}O_{3-\delta}$–YSZ ($x$ = 0.1, 0.2, 0.3) (a) at 973 K and (b) at 1073 K with Ce supported Pd catalyst (open symbols designate *V* and closed symbols designate power density). Data obtained in humidified (3% H_2O) H_2.

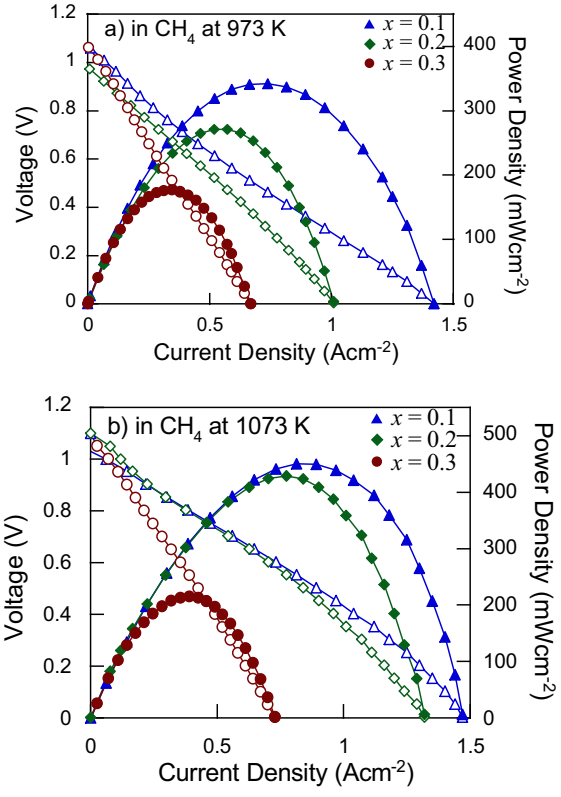

Fig. 6. *V–i* polarization curves for cells having anodes prepared by infiltration of 40 wt% $La_{0.8}Sr_{0.2}Sc_xMn_{1-x}O_{3-\delta}$–YSZ ($x$ = 0.1, 0.2, 0.3) (a) at 973 K and (b) at 1073 K with Ce supported Pd catalyst (open symbols designate *V* and closed symbols designate power density). Data obtained in humidified (3% H_2O) CH_4.

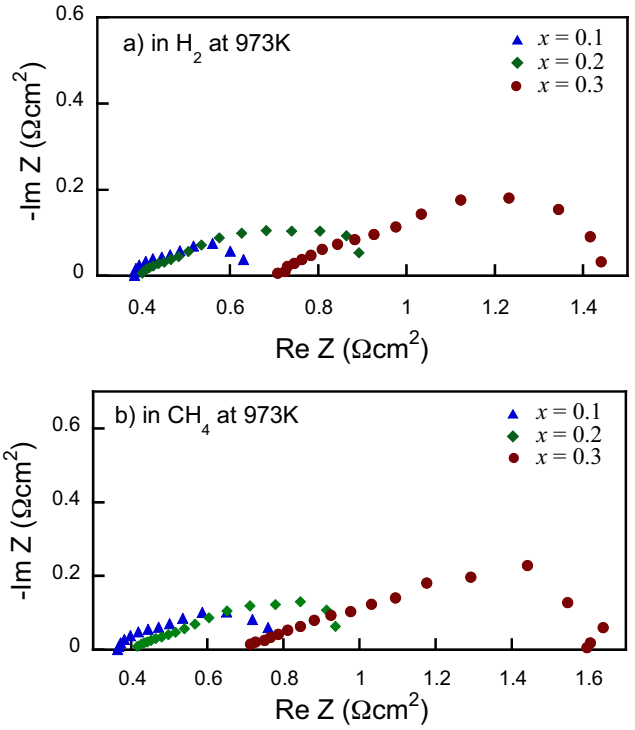

Fig. 7. Impedance spectra for cells having anodes prepared by infiltration of 40 wt% $La_{0.8}Sr_{0.2}Sc_xMn_{1-x}O_{3-\delta}$–YSZ ($x$ = 0.1, 0.2, 0.3), with Ce supported Pd catalyst into 65% porous YSZ (a) humidified (3% H_2O) H_2 fuel, (b) humidified (3% H_2O) CH_4 fuel at 973 K.

is a combination of anode and cathode impedances. The cathode impedance for the LSF–YSZ composite prepared by infiltration has been reported to be, approximately 0.1 Ω cm^2 at 973 K [18]. Considering this, it is estimated that the anode impedance for LSS01M–YSZ composite is 0.4 Ω cm^2 for methane oxidation.

To understand the catalytic activity of the LSSM–YSZ composite anode for methane combustion, identical fuel cells prepared without catalyst Ceria and Pd were examined because ceria supported Pd is a highly active catalyst for methane oxidation [19]. The *V*–*i* polarization curve for a cell prepared without catalyst is shown in Fig. 8. In general, the oxidation mechanism of CH_4 on the anode is a complex reaction. The open-circuit voltage (OCV) of these cells is near to the theoretical Nernst potential, 1.1 V in H_2 fuel. On the other hand, the observed OCV of 0.55 V in CH_4 fuel

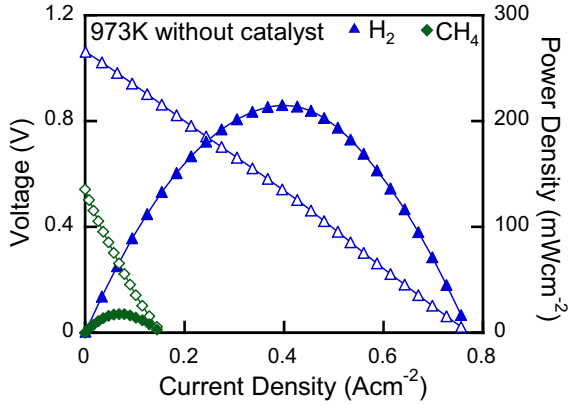

Fig. 8. *V*–*i* polarization curves for cells having anodes prepared by infiltration of 40 wt% LSS01M, without Ce supported Pd catalyst (Open symbols designates *V* and closed symbols designates power density). Data obtained in humidified (3% H_2O) H_2 (▲) and CH_4 (♦) at 973 K.

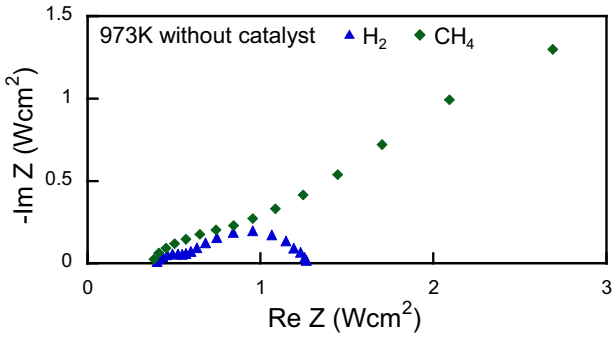

Fig. 9. Impedance spectra for cells having anodes prepared by infiltration of 40 wt% LSS01M, without Ce-supported Pd catalyst into 65% porous YSZ. Data obtained in humidified (3% H_2O) H_2 (▲) and CH_4 (♦) at 973 K.

is much lower than the theoretical Nernst potential. The low OCV might be explained by the partial oxidation of CH_4 due to the poor catalytic activity of the LSS01M–YSZ composite anode towards CH_4 oxidation. The performance of LSS01M–YSZ composite without catalysts is less than 30 mW cm^{-2} in methane fuel, which is too low. The performance of the cell with ceria-supported Pd exhibits better performance, namely, 395 mW cm^{-2}. The impedance data in Fig. 9 correspond to the data in Fig. 8 at OCV for the cells without catalyst. The impedance data show that the ohmic losses for this cell are 0.45 Ω cm^2 and are in good agreement with the expected loss for a 85 μm thick electrolyte. The large difference is in the non-ohmic losses for the cells with and without catalysts. The electrode losses in the cells with ceria supported Pd are much lower than that of the cells without catalysts as expected. LSSM-YSZ performance was improved by the infiltration of 1-wt% Pd and 10-wt% ceria. The quantity of catalytic metal infiltrated in the LSSM-YSZ electrode appears to be insufficient to afford considerable conductivity in the composite electrode for methane combustion. The added catalytic metals are inherent in TPB sites and promote oxidation of methane fuel with oxygen ions coming all the way through electrolyte. The performance of the LSSM–YSZ composite anode for methane oxidation is superior to the recently reported LSSM symmetric cell [12]. In the reported LSS02M symmetric cell, the anode is a bulk material following a conventional fabrication technique, and delivers a power density of 100 mW cm^{-2} at 1123 K. The results reported here show that infiltration of LSS01M in a porous YSZ anode with a catalyst leads to a considerable enhancement in fuel cell performance with a peak power density of 341 mW cm^{-2} at 973 K.

The microstructure of the LSSM–YSZ composite and the location of catalyst metal atoms seem to be more efficiently accomplished by the infiltration. On the other hand, the migration of the metal atoms is thought to be restricted to TPB sites in the conventional bulk anode. In LSSM–YSZ composite anode, catalytic activity is provided mostly by ceria for methane oxidation and electrical conductivity is given by the LSSM–YSZ composite. The excellent performance of the electrolyte-supported cell observed in this study may be attributed to the combined property of a thin YSZ film with low electrolyte ohmic losses and low polarization due to the improved microstructure by the infiltration technique. Composites with catalyst prepared by infiltration extensively show long TPB lengths for fuel oxidation. Among the investigated LSSM–YSZ composite anodes, LSS01M demonstrates the best performance with the lowest anode polarization resistance because of the higher electrical conductivity at 973 K.

4. Conclusion

This study shows that the anode performance can be improved by the addition of LSSM to a porous YSZ back bone via infiltra-

tion. The LSSM oxides are stable and provide excellent performance as IT-SOFC anodes operating on CH_4 as fuel. In a reducing atmosphere under anode operating conditions, LSS01M oxide shows an electric conductivity of 0.48 S cm^{-1}, which is adequate for efficient current collection and electron transfer. This material has high stability over wide range of $p(O_2)$ and the oxygen non-stoichiometry is reduced from 3 to 2.84 at 973 K. The electrical conductivity of LSSM oxides shows a dependence on $p(O_2)$ and the increase in electrical conductivity with $p(O_2)$ can be explained by an electron-hopping mechanism. An electrolyte-supported cell equipped with a 40 wt% LSS01M anode along with a ceria-supported Pd catalyst and a LSF cathode delivers a peak power density of 395 and 340 mW cm^{-2} when H_2 and CH_4 are used as fuels at 973 K, respectively. LSS02M shows 341 and 272 mW cm^{-2} and LSS03M shows 198 and 177 mW cm^{-2} when H_2 and CH_4 are used as fuels at 973 K, respectively. All of these results indicate that $La_{0.8}Sr_{0.2}Sc_xMn_{1-x}$–YSZ ($x = 0.1$, 0.2) composites with YSZ as electrolyte have great potential for application as anode material in IT-SOFCs. It is also found from coulometric titration that the stability is increased with Sc doping, as expected.

Acknowledgements

This research was supported by WCU (World Class University) program (R31-2009-000-20012-0) and Basic Science Research Program (2010-0017145) through the National Research Foundation of Korea funded by the Ministry of Education, Science and Technology.

References

[1] H. He, J.M. Hill, Applied Catalysis A: General 317 (2007) 284–292.
[2] B.C.H. Steele, I. Kelly, H. Middleton, R. Rudkin, Solid State Ionics 28–30 (1988) 1547–1552.
[3] S. Tao, J.T.S. Irvine, Nature Materials 2 (2003) 320–323.
[4] E.P. Murray, T. Tsai, S.A. Barnett, Nature 400 (1999) 649–651.
[5] G. Kim, S. Lee, J.Y. Shin, G. Corre, J.T.S. Irvine, J.M. Vohs, R.J. Gorte, Electrochemical and Solid-State Letters 12 (2009) B48–B52.
[6] S. Lee, G. Kim, J.M. Vohs, R.J. Gorte, Journal of The Electrochemical Society 155 (2008) B1179–B1183.
[7] S. Tao, J.T.S. Irvine, Journal of The Electrochemical Society 151 (2004) A252–A259.
[8] T. Kolodiazhnyi, A. Petric, Journal of Electroceramics 15 (2005) 5–11.
[9] G. Corre, G. Kim, M. Cassidy, J.M. Vohs, R.J. Gorte, J.T.S. Irvine, Chemistry of Materials 21 (2009) 1077–1084.
[10] P. Zeng, R. Ran, Z. Chen, W. Zhou, H. Gu, Z. Shao, S. Liu, Journal of Alloys and Compounds 455 (2008) 465–470.
[11] P. Zeng, R. Ran, Z. Chen, H. Gu, Z. Shao, S.S. Liu, AIChE Journal 53 (2007) 3116–3124.
[12] Y. Zheng, C. Zhang, R. Ran, R. Cai, Z. Shao, D. Farrusseng, Acta Materialia 57 (2009) 1165–1175.
[13] J.W. Erning, T. Hauber, U. Stimming, K. Wippermann, Journal of Power Sources 61 (1996) 205–211.
[14] S. Yoo, J.Y. Shin, G. Kim, Journal of Materials Chemistry 21 (2010) 439–433.
[15] J. Mizusaki, N. Mori, H. Takai, Y. Yonemura, H. Minamiue, H. Tagawa, M. Dokiya, H. Inaba, K. Naraya, T. Sasamoto, T. Hashimoto, Solid State Ionics 129 (2000) 163–177.
[16] H. Gu, Y. Zheng, R. Ran, Z. Shao, W. Jin, N. Xu, J. Ahn, Journal of Power Sources 183 (2008) 471–478.
[17] K. Sasaki, J. Maier, Solid State Ionics 134 (2000) 303–321.
[18] Y. Huang, J.M. Vohs, R.J. Gorte, Journal of The Electrochemical Society 151 (2004) A646–A651.
[19] S. Colussi, A. Trovarelli, G. Groppi, J. Llorca, Catalysis Communications 8 (2007) 1263–1266.